Atmos. Meas. Tech. Discuss., 2, 3183–3220, 2009
www.atmos-meas-tech-discuss.net/2/3183/2009/

Atmospheric Measurement Techniques Discussions

This discussion paper is/has been under review for the journal Atmospheric Measurement Techniques (AMT). Please refer to the corresponding final paper in AMT if available.

Ground-based observations for the validation of contrails and cirrus detection in satellite imagery

H. Mannstein[1], **A. Brömser**[1,2], **and L. Bugliaro**[1]

[1]Deutsches Zentrum für Luft- und Raumfahrt, Institut für Physik der Atmosphäre, Oberpfaffenhofen, Germany
[2]UBIMET GmbH, 1200 Wien, Austria

Received: 23 November 2009 – Accepted: 26 November 2009
– Published: 10 December 2009

Correspondence to: H. Mannstein (hermann.mannstein@dlr.de)

Published by Copernicus Publications on behalf of the European Geosciences Union.

Abstract

Contrails and additional cirrus clouds caused by air traffic have a potential warming effect due to their optical properties and their location in the upper troposphere. The effect of contrails is directly related to their coverage and optical properties, which can be derived from satellite observations, but considerable local and global uncertainties remain, as detection limits and efficiency are still unknown. A 6 months time series of the occurrence of high-level clouds and contrails was analysed visually from an all-sky camera situated at Oberpfaffenhofen (Southern Germany). It shows a contrail occurrence (fraction of time with visible contrails during one hour) of 21% being nearly constant over daytime and a cirrus occurrence that increases from 27% in the morning to 48% in the evening, suggesting a possible influence of air traffic or, more probably, convection. Furthermore, we compared selected all-sky camera images with data of the satellite instruments NOAA/AVHRR and MSG/SEVIRI. As expected, the fraction of contrails visible and detectable in satellite images depends highly on their width. Of the contrails observed with the all-sky camera being 1–5 km wide, 60–65% are visually detectable in AVHRR data, while only 17% are identified by an automated contrail detection algorithm (CDA). However, the CDA detects approx. 28% of the visually detected contrails. As far as SEVIRI is concerned, visual inspection yields 48% of the contrails of 1–5 km width, the CDA 19%. This value rises to 40% when comparing to the visually detected contrails. As far as cirrus detection with SEVIRI is concerned, an automated algorithm tends to overestimate cirrus occurrence but correctly appraises cirrus changes during the day.

1 Introduction

Contrails (short for condensation trails) have been observed since 1915 (Schumann, 2005), the theory of the thermodynamic conditions causing their formation and decay was developed at the time of World War II (Schmidt, 1941). The frequent occurrence of

AMTD

2, 3183–3220, 2009

contrails due to the strong growth of global air traffic has triggered intensive research in this field since the early 1990s, especially with respect to their present and future influence on global and regional climate (Meerkötter et al., 1999; Mannstein et al., 1999; Meyer et al., 2002; Marquart, 2003; Minnis et al., 2004).

Aircrafts add warm and humid exhaust to the tropopause region. When the plume consisting of exhaust and entrained air cools, its relative humidity increases. If the ambient air is cold and moist enough, saturation with respect to liquid water will be reached, which is the necessary condition for the formation of an exhaust contrail. The temperature and moisture limits are given by the Schmidt-Appleman Criterion (Schmidt, 1941; Appleman, 1953; Schumann, 1996). In warmer and moist surroundings contrails can also be initiated aerodynamically (Gierens et al., 2009; Kärcher et al., 2009). If the ambient air is supersaturated with respect to ice the contrail can persist for several hours. Live spans of more than 7 h for single contrails and 17 h for contrail clusters (Minnis et al., 1998) together with contrail widths of 15 km have already been observed, but usually the contrail loses its linear appearance and cannot be distinguished by its shape from a naturally formed cirrus cloud after 1 or 2 h (Mannstein et al., 1999).

The most relevant parameters to estimate the climate impact of contrails are changes in cirrus cloud coverage, optical thickness, the resulting radiative forcing (RF) and possible effects due to change of air composition and influence on the hydrological cycle (Schumann, 2005). Like thin cirrus, contrails reduce both the incoming short wave radiation and the infrared radiation escaping into space (greenhouse effect). The former effect leads to an instantaneous surface cooling during daytime, the latter causes a warming mainly of the upper troposphere.

Cirrus cloud amount is on the one hand modified by contrails detectable due to their linear structure, on the other hand by additional contrail cirrus clouds that can only be detected indirectly by observing changes in cirrus cloud coverage. The global coverage of contrails is estimated to be in the range between 0.04% and 0.09% (Stuber and Forster, 2007), in Central Europe it amounts to 0.5 ±0.25% with regional maxima

AMTD
2, 3183–3220, 2009

reaching 1.2% (Mannstein et al., 1999). The coverage of aviation-induced cirrus is estimated to be 1.8 to 10 times higher than the one caused by contrails (Forster et al., 2007). According to Stordal et al. (2005) cirrus coverage in Europe increased by 1–2% per decade, Zerefos et al. (2003) find a value of 1.8% for Europe. The optical thickness of contrails on global average lies between 0.15 and 0.25 (Minnis et al., 2005), Meyer et al. (2002) found a lower value of 0.1 for Europe. The radiative forcing caused by contrails is estimated to be in between 3.5 and 17 $mW\,m^{-2}$ using air traffic conditions of 1992 (Schumann, 2005), in the current IPCC report (IPCC, 2007) it is estimated to be in between 3 and 30 $mW\,m^{-2}$, the best estimate being 10 $mW\,m^{-2}$ for both the years 2000 and 2005 (Forster et al., 2007). According to Stordal et al. (2005) the RF of the additonal cirrus ranges in between 10 and 80 $mW\,m^{-2}$ with a best estimate being 30 $mW\,m^{-2}$. In a new assessment Lee et al. (2009) give an estimate of 12 $mW\,m^{-2}$ for the linear contrails and 33 (11–87) $mW\,m^{-2}$ for aviation indiced cirrus. At present the influence of additional, aircraft-induced aerosol particles which might have an impact on cirrus coverage ("soot cirrus") on the Earth radiation budget cannot be quantified (Forster et al., 2007).

We present the analysis of 6 months of data from the all-sky camera "Wolkam" (this name stands for German "Wolkenkamera" meaning cloud camera), situated on the roof of the Institute of Atmospheric Physics located at the DLR Campus at Oberpfaffenhofen close to Munich. This is a region of heavy air traffic in the heart of Europe at a distance of approximately 50 km South-West of Munich Airport. From the nearly complete time series from April to September 2007 we derived monthly means and diurnal cycles of contrail and cirrus occurrence. These were compared to satellite data from NOAA/AVHRR and MSG/SEVIRI in order to estimate contrail detection efficiency at the location of the all-sky camera. Furthermore we determined the minimum width that is needed for a contrail to be detected in NOAA/AVHRR and MSG/SEVIRI satellite imagery. Thereby, data from these two space-borne instruments was analysed both visually and by means of the contrail detection algorithm developed by Mannstein et al. (1999). Cirrus detection from MSG/SEVIRI data was performed by use of the MeCiDA

algorithm described in (Krebs et al., 2007) and compared to Wolkam data as well.

After a description of the all-sky camera and a short illustration of the satellite radiometers main characteristics in Sect. 2, the visual inspection methods and the algorithms used as well as the intercomparison details are explained in Sect. 3. Section 4 presents the monthly time series and the diurnal cycles of cloud occurrences extracted from the all-sky camera as well as the resulting contrail width distribution. The intercomparisons between Wolkam and AVHRR or SEVIRI are shown in Sects. 5 and 6 respectively, together with the estimation of the contrail detection efficiency and of the MeCiDA performance. Finally, conclusions are drawn in Sect. 7.

2 Instruments

2.1 The Wolkam all-sky camera

For ground-based contrail observations all-sky cameras are suitable (Sassen, 1997) because they are capable of covering almost the whole visible sky by the use of fisheye lenses and offer high temporal resolution (several images per minute). The Wolkam camera houses a CCD sensor providing colour images having a size of 2040×2040 pixels (32 MB in tiff format). The all-sky camera holds a 17 to 28 mm fisheye zoom objective yielding images with an opening angle of 90° to 180°. In this study the minimum focal length is used resulting in the maximum viewing angle of 180°. These images cover all the visible sky except some areas close to the horizon, which is due to the square shape of the CCD chip. A neutral optical filter is used to damp direct sunlight. The optics and electronics are placed in a waterproof housing, the objective is located in the centre of an acrylic dome. Exposure time is automatically adapted to the prevailing light conditions by averaging the brightness of the whole image area of the proceeding images and adjusting it to a target value, shutter speeds in the range of 25 ms to 130 s are possible.

AMTD
2, 3183–3220, 2009

Routinely, the image is compressed to a 512×512 pixels jpg file of about 50 kB size, and the original tiff file is deleted. Approximately six such jpgs are obtained every minute during daylight time, usually this process proceeds automatically without interruption. If an all-sky camera image is gathered within 30 s of a NOAA satellite overflight time, the original high-resolution tiff files are kept.

All the images of the Wolkam camera are considerably distorted because of the wide angle optics. To make a comparison to satellite images possible, they have been deskewed, mapped on a plane, and aligned to the cardinal points. This enables the correct determination of the geographical location and the size of the contrails. However, to get accurate results, the height of the contrails above ground level has to be known. In this study it was assumed to be 10 000 m, the usual cruise altitude. The used mapping routine produced images with a resolution of 75 m/pixel yielding squarish images with an edge length of about 38 km where at least all parts of the sky with a zenith angle smaller than 62° are displayed. A comparison of an unmapped and a mapped image is shown in Fig. 1e and f.

The all-sky camera worked with only short interruptions from April to September 2007 for a total of evaluable 2549.1 h. This time series was inspected visually since an automatic image interpretation scheme was not possible due to artefacts like blooming of a significant part of the image caused by the sun, improper focusing or reflections within the optical system, morning dew on the acrylic dome.

This visual inspection was performed by a single individual to guarantee consistency of the resulting data set. However, to exclude gross subjective misinterpretations of the camera images, a test has been conducted where four observers investigated a five day subset of the Wolkam data. This demonstrated that a certain amount of subjectiveness is present but that altogether a satisfactory agreement was found.

2.2 NOAA/AVHRR and MSG/SEVIRI

The SEVIRI radiometer (Schmetz et al., 2002) of the geostationary MSG-2 satellite, situated at 0° E longitude, provides an image of the whole visible surface of the Earth

in 12 spectral channels every 15 min. Its spatial resolution at the subsatellite point amounts to 3 km in all but one channel, the HRV (High Resolution Visible) channel, which has a spatial resolution of 1 km.

The period of revolution of the polar-orbiting sun-synchronous NOAA satellites is about 102 min, their altitude being around 850 km. The AVHRR/3 (Goodrum et al., 2003) radiometer aboard them features 6 spectral channels, a nadir spatial resolution of 1.1 km and a swath width of about 2500 km. Data from NOAA12, NOAA14, NOAA17, and NOAA18 acquired at the German Remote Sensing Data Centre of DLR in Oberpfaffenhofen, Germany, was used. At the times of 49 NOAA overpasses (19 of NOAA12, 0 of NOAA14, 11 of NOAA17 and 19 of NOAA18) contrails have been observed in the camera images. The total number of AVHRR overpasses over Oberpfaffenhofen during the investigated time period amounted to 600–700.

3 Methods

3.1 Visual evaluation of Wolkam data

Every image of the all-sky camera has been classified according to five basic categories:

1. *Low- and medium-level clouds*: The visibility of the cirrus and therefore the contrail level is blocked or considerably limited by low- and medium-level clouds: according to experience the sky will be classified in this category, if more than 5 to 6 oktas of the sky is covered with these clouds.

2. *Contrails without cirrus*: There are contrails but no natural cirrus clouds in the field of view of the camera (the simultaneous appearence of cirrus and spatially clearly separated contrails belong to this category and to category 4 at the same time; however, this does not really affect statistics due to its extremely rare occurrence).

Natural cirrus here means that it cannot be visually classified as a contrail, but this does not exclude formation initiated by contrails.

3. *Contrails and cirrus*: Contrails and cirrus clouds, which are not clearly spatially separated, appear both in the field of view.

4. *Cirrus without contrails*: Natural cirrus clouds, but no contrails are visible (the rare simultaneous occurrence of cirrus and spatially clearly separated contrails belongs to this category and to category 2 at the same time). Again, natural cirrus means that it cannot be visually classified as a contrail.

5. *Cirrus level visible, neither cirrus nor contrails*: The images which do not belong to any other category, meaning the sky is devoid of clouds or there are low- or medium-level clouds covering less than about 5 oktas of the sky.

In order to obtain the whole time fraction (i.e. relative frequency of occurrence) of the appearance of contrails or cirrus, three combined categories were added:

6. *All contrails*: Sum of "Contrails without cirrus" and "Contrails and cirrus".

7. *All cirrus*: Sum of "Contrails and cirrus" and "Cirrus without contrails".

8. *All ice clouds*: Sum of "All cirrus" and "Contrails without cirrus" (same as sum of "All contrails" and "Cirrus without contrails").

It has to be emphasised that the use of the illustrated procedure does not determine the cloud amount, the classification in the categories is always a binary decision ("yes" or "no") for every image.

The first occurrence time of a cloud category and the last occurrence time were recorded. The accuracy of the determination of these points in time is limited by several factors like slowly changing cloud structures (e.g. gradual transformation from cirrostratus into altostratus), broken cloud layers or the non-consideration of clouds appearing

very close to the horizon. Because of this the times were determined with an accuracy of five minutes except for short-lived contrails.

Only those contrails were regarded that could be identified in the images for at least three minutes. The consideration of all the contrails would greatly have increased the number of points in time to be noted without changing the relative frequencies of the categories by much. Furthermore the short-lived and thus narrow contrails would not be detectable in satellite imagery anyway.

Finally, hourly sums of these cloud situations were computed. The frequencies were calculated in relation to the actual complete measurement period (all the daylight hours without the times of data loss caused by problems with the camera system and morning dew) as well as in relation to the period of visible cirrus level.

The sampling error, i.e. the uncertainty caused by considering only a limited sample of independent observations instead of the whole population is defined as $\sigma_n = \sigma/\sqrt{n}$. Here σ =0.5 because only binary decisions occur. n denotes the size of the sample, which was fixed by determining the amount of uncorrelated images. It was assumed that it takes 20 min for low- and medium-level clouds and 30 min for high-level clouds until the pictures are no longer correlated. These time spans were estimated by visual inspection of approximately one dozen cloud scenes. The size n of the sample is identified by calculating the number of uncorrelated Wolkam scenes using the whole measurement period within the particular time span, e.g. a month. If the sampling error exceeded 5% the data was not considered.

3.2 AVHRR vs. Wolkam

In the Wolkam image data corresponding to the AVHRR overpass times 96 contrails could be visually detected, whereas the period was slightly extended backwards in time to 23 March 2007 in order to increase their number. AVHRR overflights where associated Wolkam images showed neither contrails nor cirrus where discarded. At the same time, the automatic contrail detection algorithm (CDA) developed by Mannstein et al. (1999) was applied to the satellite data in order to extract linear structures from

brightness temperature difference (channel 4 – channel 5) and brightness temperature (channel 5) images. An interesting but atypical case is represented by the NOAA overpass on 16 April 2007 at 12:02 UTC (Fig. 1). Here, 11 contrails could be observed at the same time (while usually only one contrail was found over Oberpfaffenhofen at the time of a NOAA overpass). Besides to the CDA results (Fig. 1d), additional AVHRR data is considered: channel 5 brightness temperatures (Fig. 1a), which display contrails as dark, linear structures embedded in a brighter (warmer) background, brightness temperature differences (channel 4 – channel 5), where contrails (Fig. 1b) appear as bright lines contrasting a darker background, and false colour composites (Fig. 1c: channel 1, 2 and 5 with contrails as light blue structures on top of an inhomogeneous background). Obviously especially the young and therefore thin contrails are emphasised in the brightness temperature difference image (Inoue, 1985) which enables the observer to even detect contrails which are not visible in the Wolkam images. In contrast, some aged and thus wide contrails are detectable in the Wolkam images but not in the temperature difference image. This brightness temperature difference is used as a thin cirrus test in remote sensing of clouds. For transparent ice clouds it increases with decreasing particle size.

In order to facilitate the comparison to the Wolkam images, the AVHRR data was first deskewed, the vicinity of the all-sky camera location was clipped and enlarged and a circle with a radius of 25 km to enable the orientation within the AVHRR scene was centred at Oberpfaffenhofen (Fig. 1a–d).

Detection due to the CDA was considered successful if it identified a contrail within the circle drawn around Oberpfaffenhofen that could be visually confirmed using the all-sky camera (Fig. 1e). In the example, out of the 11 numbered contrails visible in the all-sky camera image only 3 of them are detectable in channel 5 temperatures, 7 in the temperature difference image, 2 in both the false colour composite and the CDA result.

The assessment of the contrail width in the all-sky camera was based on the assumption that one pixel of the mapped camera image corresponds to 75 m when the contrails are situated 10 km above the ground. The deviation from the real flight level

AMTD
2, 3183–3220, 2009

is smaller than 2 km in more than 90% of all cases according to a diagram published by Fichter et al. (2005). This results in a pixel width error smaller than 15 m for 90% of all cases. Assuming a starting width of 60 m and a rate of broadening of 50 m min^{-1} (values taken from Mannstein et al. (1999)), this width is already reached after one minute. This implies the possibility of observing almost all contrails using an all-sky camera, especially if difference images of two consecutive shots separated in time by several seconds are used to accentuate thin contrails.

Subsequently, the contrails were divided into five classes according to their width to investigate the relationship between width and detection efficiency (for this the efficiency of the all-sky camera is set to 100%). Finally, the brightness temperature difference between every contrail being detectable in both the all-sky camera and the AVHRR image and its surrounding area was determined. This difference was used to estimate the contrail optical thickness by Meyer et al. (2002).

3.3 SEVIRI vs. Wolkam

The CDA originally developed for AVHRR has been recently adapted to MSG/SEVIRI and applied to the 2797 MSG-2 slots of May 2007, a month with frequent occurrence of contrails. This dataset could be used to determine contrail occurrence to compare to the Wolkam time series of the corrsponding "All contrails" class. For an additional CDA validation on SEVIRI, a visual analysis was performed in analogy to that for AVHRR (Sect. 3.2) by comparing the Wolkam images to SEVIRI brightness temperature differences (channel 7 – channel 10), SEVIRI false colour composites (using channels 1, 2, 10, and 12) and the output of the CDA on SEVIRI. Again, SEVIRI data were cropped to an area of 48×24 pixels resembling Southern Germany and the borders of the Wolkam area were marked. The situations showing contrails in the SEVIRI image but not in the all-sky camera image were left without consideration. The width of the contrails was again determined under the assumption of a contrail height of 10 km above ground. However, this additional visual analysis was restricted to the SEVIRI data of Southern Germany gained at minute 56, avoiding multiple consideration of the same contrail as

it takes typically more than 15 but less than 60 min to traverse the Wolkam camera's field of view. In the corresponding Wolkam dataset 79 contrails could be identified.

Furthermore, the Meteosat Second Generation Cirrus Detection Algorithm (MeCiDA) algorithm (Krebs et al., 2007) was applied to SEVIRI to determine the occurrence of cirrus clouds in the all-sky camera's field of view with high temporal resolution (15 min) during the full six month period. MeCiDA decides wether a SEVIRI pixel is cirrus covered by means of several threshold and morphological tests based on thermal channels alone. Since it turned out that for some reason almost always single pixels were classified as cloudy by MeCiDA inside the area of interest, we decided to build our analysis on a smaller area of 9×9 pixels around the all-sky camera: The larger 48×24 pixel area was first inspected to better identify cirrus structures, but the final decision about cirrus cloud occurrence was based upon the smaller region alone. The results of MeCiDA for the 81 SEVIRI low resolution pixels corresponding to the area covered by the all-sky camera observations were used in two ways: 1) analogously to the analysis of the Wolkam time series, cirrus clouds and contrails (which are undistinguishable for MeCiDA) appeared if at least one of the pixels was classified as covered with cirrus; 2) cirrus cloud coverage was calculated considering the 81 SEVIRI pixels corresponding to the all-sky camera observations. In addition, visual analysis of SEVIRI false colour composites and brightness temperatures was performed and the relative frequencies of cirrus clouds occurrence determined. To make the comparison of the SEVIRI and Wolkam data sets possible, the SEVIRI products were aggregated for each hour of the day.

4 Ground-based observations of cirrus and contrails

4.1 Monthly variations of cirrus and contrail occurrence

The monthly distribution of the categories 1–4, 6, 7 (Sect. 3.1) relative frequencies in relation to the whole measurement period is presented in Fig. 2 (left). The frequency

AMTD
2, 3183–3220, 2009

of “All contrails” occurrence fluctuates between 6% in July 2007 and almost 20% in April 2007 with a mean value of 12%, the one of “All cirrus” features a maximum of 27% in May and a minimum of 11% in September (mean value 20%). A positive correlation of both classes is suggested by the grafics, the expected negative correlation to “Low- and medium-level clouds” is also observable. The remarkable small frequency of the last-mentioned category in April 2007 (11%) is due to the unusually sparse occurrence of cloudy conditions in this month. Its continuous increase from April to September is related to the general weather situation peculiar to that particular year. Remember by the way that low clouds are assigned to this category only if they fill at least 5 to 6 oktas of the sky (see Sect. 3.1).

Figure 2 (right) displays the monthly frequency of occurrence of the “Contrails and cirrus”, “All contrails” and “All cirrus” categories with respect to the time span where the cirrus level was visible from the ground. Of course, values are larger than in Fig. 2 (left). The “All contrails” line varies from 11% in July to 31% in May, and averages to 21%. The “Contrails and cirrus” follows quite closely the previous one at a somewhat lower level, while the “All cirrus” line ranges between 26% in July and 45% in May and June, its average being 35%. The fluctuations of these cloud categories are presumably due to changes of the large scale weather pattern, but their apparent positive correlation suggests that when the conditions for cirrus formation and persistence are given (supersaturated air parcels) this also affects contrail formation. Compared to Wylie et al. (2005, Fig. 4), where the monthly frequency of high clouds (above 6 km) in the 20°–60° N latitude belt derived from HIRS (High Resolution Infrared Radiation Sounder) aboard the NOAA satellites lies between 25 and 35% in the early 2000s, a reasonable agreement is found. Due to the HIRS lower sensitivity to thin cirrus, these values are smaller than those derived from the SAGE (Stratospheric Aerosol and Gas Experiment) II limb sounder (Wylie and Wang, 1997), while they are higher than those obtained from ISCCP (Jin et al., 1996). The TOVS Path-B dataset (Scott et al., 1999) yields instead frequencies of cirrus clouds in northern midlatitudes of about 25%, and Hahn and Warren (2007) mention a frequency of high clouds over land of 45% from

surface observations between 1971 and 1996. Ground measurements at Hohenpeissenberg, Germany, (some 50 km from DLR Oberpfaffenhofen) show cirrus frequencies between 40 and 70% in the late 90 s as a function of month (Trepte and Winkler, 2001).

4.2 Diurnal cycle of cirrus and contrail occurrence

Because of the restriction to daylight and the non-consideration of hours with a sampling error exceeding 5%, the diurnal cycle is investigated between 04:00 UTC and 19:00 UTC. In the plots, the 04:00 UTC occurrence represents the occurrence between 04:00 and 05:00 UTC, and so on.

Figure 3 (left) depicts time percentages relative to the whole measurement period. The frequencies of occurrence of the category "Low- and medium-level clouds" first decline from 56% (04:00–05:00 UTC) to 37% (14:00–15:00 UTC) then slightly increase to 45% (18:00–19:00 UTC) over the course of the day. Surprisingly, the onset of (cumulus) convection due to increasing solar insolation is not observable in the data set. On one side, this is due to the very definition of category 1 "Low- and medium-level clouds" where at least 5 to 6 oktas of the sky must be covered by clouds. On the other side, the effect of convection on this cloud class is masked by other processes like the dissipation of low stratiform clouds with increasing solar insolation during the course of the day. The contrail occurrence does not show a significant diurnal cycle, it fluctuates between 8% and 14%. This agrees well with the fact that air traffic density over Central Europe is very low at night, increases very rapidly between 02:00–03:00 UTC and 07:00–08:00 UTC and remains then stable until 21:00 UTC when it decreases again (Fig. 4). In contrast, a considerable cirrus cloud diurnal cycle exists: "All cirrus" frequence increases almost continuously from 11% (05:00–06:00 UTC) to 29% (17:00–18:00 UTC). The "All ice clouds" class behaves similarly, passing from 16% in the morning to 31% in the afternoon. The frequencies relative to the period with visible cirrus level are displayed in Fig. 3 (right). Again the contrails do not indicate a diurnal cycle, their frequency of occurrence oscillates between 16% and 26%. The cirrus clouds reveal a significant diurnal cycle: their frequencies rise from 23% (05:00–06:00 UTC) to

48% (17:00–18:00 UTC). After an increase by 10% to 30% in the first morning hours, the "All ice clouds" occurrence remains more or less stable until 14:00–15:00 UTC and eventually increases again by 10% to 50% (17:00–18:00 UTC).

The cirrus cloud increase could be caused by either natural or anthropogenic cirrus cloud formation mechanisms, or by both of them. The main natural source of cirrus clouds during the spring-summer season is certainly convection that is usually initiated in the afternoon. The main anthropogenic source of cirrus clouds, air traffic, affects ice cloud formation through contrails: during the course of the day more and more contrails could evolve into cirrus clouds, while during nighttime this cirrus would eventually have the time to dissipate while few contrails are produced due the very small air traffic density (Fig. 4). Since it is not possible to quantify the amount of cirrus clouds produced by convection, we consider air traffic density *Dtr* shown in Fig. 4 to estimate the probability that at least one aircraft is within the Wolkam visible range. We assume a mean aircraft speed V of 850 km/h, a visible area with a radius R of 35 km and a Poisson distribution (rare events) for the probabilities that N aircrafts are within this area. Then, the probability $P0$ that no aircraft is visible reads $P0 = \exp(-Dtr * \pi * R^2/V)$ and the probability that at least one aircraft is visible $P1 = 1 - P0$. This probability does not change much during daylight time (Fig. 4) and follows the curve of air traffic density. An aircraft crosses the area in approx. 4 min, which defines the auto-correlation time scale. Thus, the probability that an aircraft crosses the Wolkam field of view within 10 min is constantly equal to unity between 04:00 and 21:00 UTC. We can first conclude that the weather situation, i.e. the probability of ice supersaturation at the flight levels, and not the air traffic density determines (i.e. limits) the occurrence of contrails at daytime over Southern Bavaria. Secondly, from the observation that the occurrence of at least three minutes old contrails (see Sect. 3.1) is more or less constant over the day and from the constancy of the probability of seeing an airplane we can conclude that the probability of ice supersaturation at the flight levels does not significantly change during the day. However, implications about the vertical extension of such supersaturated regions cannot be drawn since air traffic mainly takes place in a very limited number

of flight levels. Thus, the onset of convection in the afternoon could lead to more frequent cirrus formation and enhanced cirrus occurrence in (mainly lower) atmospheric levels during the course of the day. The strong daytime increase of cirrus occurrence in Wolkam images is also accompanied by an increase in cirrus cover as shown in Fig. 7. A second explanation for this increase might be the advection of contrail cirrus initiated hours before.

4.3 Contrail width

The widths of all contrails, including very short-lived ones, being visible in all-sky camera images (Sect. 3.2) at the times of NOAA overflights were determined from Wolkam images. This will enable in Sects. 5 and 6 to estimate the minimum width needed for contrails to be detectable in AVHRR or SEVIRI images. This sample consists of all 96+79 contrails found in Wolkam data as illustrated in Sect. 3.2 and 3.3. It was divided into five width classes according to Fig. 5.

This figure reveals that contrails of the categories <0.5 km (29%), 0.5–0.9 km and 1.0–1.9 km (27% each) occur almost equally frequently, their fraction diminishes considerably towards bigger widths, just 5% are more than 5 km wide (however, some of the broader contrails may have lost their linear shape and may have been classified as natural cirrus). The thinnest visible contrails feature a width of approximately 150 m (2 Wolkam pixels). This confirms the suitability of the all-sky camera for observing contrails as stated in Sect. 3.2.

5 Validation of AVHRR algorithms

5.1 Contrail detection efficiency

Of the 96 contrails observed in Wolkam images at the time of the NOAA overpass, 38 (40%) were identified in AVHRR channel 5 data, 40 (42%) in temperature difference

images and 23 (24%) in the false colour composites; the CDA detected 8 contrails (8%). A discrimination between the three different instruments on NOAA11, NOAA16 and NOAA17 is not possible due to the relatively small size of the sample.

Table 2 shows the detected contrails as a function of their width as determined from Wolkam data (see Sect. 4.3). The three visually interpreted image types (channel 5 temperature, temperature differences, false colour composite) exhibit an increasing detection efficiency as contrail width grows, but at large widths it decreases except in channel 5. Only one contrail thinner than 0.5 km was detectable by eye in an AVHRR temperature difference image. Although the number of contrails detected in brightness temperature and brightness temperature difference images is similar, their width distribution differ: their mean width is 2.6 km and 1.9 km respectively. On the one hand this is explicable by the occurrence of the lowest temperatures (relative to the surroundings) at the centre of wide contrails (Meyer et al., 2002), making them easily recognisable as dark lines. On the other hand the smaller ice crystals of young and thus thin contrails in comparison to cirrus clouds lead to a larger difference in emissivity, which causes them to appear as bright lines in the temperature difference images while their temperature contrast with respect to the surroundings remains small. To ensure a high detection efficiency, both information source should be utilised, as it is done in the CDA. The colour composites feature a clearly lower detection efficiency than the first two image types, the mean width of the detected contrails is 2.2 km, and the width distribution is similar to the one detected with temperature difference images. Compared to the channel 5 temperature and the temperature difference plots, false colour composites contain information from thermal as well as from solar channels. Thin cirrus however is hardly visible in solar channels because solar channels introduce additional variability of the (relatively bright) background that hinders cirrus detection.

The CDA detects less than 10% of the contrails seen on Wolkam images, their width ranging from 1 km to 5 km. Two of the eight contrails detected by the CDA could not be associated with single contrails, but only with a pair of them. These cases were counted once for the compilation of Table 2. This detection efficiency is significantly

lower than the one specified in Mannstein et al. (1999), where a value of 30–50% was found in a sensitivity study against visually inspected AVHRR data. One reason for the lower detection efficiency in relation to Wolkam is the inhomogeneous temperature distribution in the proximity of the all-sky camera location mainly caused by the urban heat island of Munich and the big lakes in the surrounding area (Lake Ammersee, Lake Starnberg). This aspect has already been investigated in Mannstein et al. (1999, Fig. 16), where the dependency of contrail cover on AVHRR channel 5 brightness temperatures inhomogeneity is estimated in order to correct CDA results in a statistical sense. In Mannstein et al. (1999, Fig. 15) the spatial distribution of AVHRR channel 5 brightness temperatures standard deviations is shown and confirms that the area investigated in this paper is particularly sensitive to this issue. However, in the present study no statistical correction in the sense of Mannstein et al. (1999) is possible. Furthermore, Mannstein et al. (1999) determined detection efficiency by comparing CDA results with contrails manually detected in AVHRR images by some human observer. In order to reproduce these conditions, we can determine the CDA detection efficiency by comparing CDA results to the other AVHRR image types used for contrail detection (channel 4 – channel 5 brightness temperature differences, channel 5 brightness temperatures and colour composites). Then, the CDA efficiency ranges from 20 to 35%, which does not largely differ from the values contained in Mannstein et al. (1999).

Finally, we consider only those contrails whose width is at least comparable to the nominal AVHRR pixel size of 1.1 km at nadir that are expected to be detected by the four methods (temperatures, temperature differences, false colour composites, and CDA), according to the explanations given above. For temperature images and false colour composites we regard all 54 contrails with a width larger than 1 km: the resulting detection efficiencies amount to 61 and 37% respectively. For the temperature differences and the CDA a new reference ensemble of 47 contrails of width 1–5 km is built: the resulting detection efficiencies amount to 62 and 17% respectively. The fact that some wide contrails are not detected visually or by the CDA is probably related to their small optical thickness.

This analysis is not only interesting because it enables to evaluate the performance of the automated CDA algorithm. It also allows to better rate investigations of contrail occurrence based on visual evaluation of AVHRR data. In particular, the pioneering work of Bakan et al. (1994) is often cited as an early source of contrail occurrence (and coverage) information and has been used to calibrate numerical model analyses of global linear contrail coverage (see for instance Sausen et al. (1998)). Bakan et al. (1994) is based on visual inspection of printed AVHRR brightness temperature images. Due to the reduced spatial resolution of the images of 20 km per mm, the authors assert that they can only detect older (thus wide) contrails, but they cannot quantify how many contrail they miss. Our investigation shows that thin narrow contrails represent the majority of the contrails observed with Wolkam and that AVHRR channel 5 temperatures enable to detect only a moderate fraction of these contrails. In fact, at least in our case, contrails smaller than 2 km make up three 78% of the detected contrails and channel 5 temperature images "contained" 32% of them. Furthermore, of the larger contrails (≥2 km), 67% are detected in channel 5 brightness temperatures. Of course, the surroundings of the Wolkam camera is particularly unfavourable with respect to contrail detection. However, the concentration to this small spot makes a more detailed inspection possible than the full AVHRR swath. Using our figures, one would estimate detection efficiency in Bakan et al. (1994) to be approximately 21%. The way how this affects contrail occurrence or contrail coverage is even more difficult to assess. Anyway, although it is very difficult to make a quantitative assertion, it is evident that only a relatively small fraction of the existing contrails could be identified by Bakan et al. (1994).

5.2 Relationship of contrail width and brightness temperature change

The brightness temperature differences between each contrail and its surrounding are plotted in Fig. 6 (left) for channel 5 temperatures and for brightness temperature differences (right). In both graphics diamonds (◊) mark single contrails, triangles (△)

indicate 2 contrails each, an asterisk (∗) at the centre marks the successful detection of the contrail by the CDA.

Regarding channel 5 temperatures, the minimum difference for a detectable contrail is 1–2 K, most differences are smaller than 10 K, the average is 5.2 K. A positive correlation between width and temperature difference is identifiable meaning that the lowest temperatures occur in the centre of wide contrails, consistently with the findings of Meyer et al. (2002). Due to the AVHRR images featuring a resolution of about 1 km, the possibility of contrails not filling a satellite pixel completely is given, especially for thin contrails (<2 km). Thus, contrail brightness temperatures are contaminated by their surrounding temperatures such that temperature differences are smaller than expected. The mean difference of 5.2 K also coincides well with the 5.4 K established by Meyer et al. (2002).

Considering the temperature difference between channel 4 and 5 (Fig. 6 (right), same meaning of the symbols), the minimum inside-to-outside-contrail contrast value is 0.2–0.3 K, the largest values are 2–3 K, the average is 0.8 K. The mentioned positive correlation is more pronounced in this case: in accordance with Meyer et al. (2002) the temperature difference increases towards the centre of wide contrails. Again, partly covered pixels induce smaller temperature diffferences and this is probably the case for thin contrails.

6 Validation of SEVIRI algorithms

6.1 Contrail detection efficiency

Of the 79 contrails identified in the all-sky camera images (Sect. 3.3), 12 of them (15%) were identifiable in the SEVIRI temperature difference images and 7 (10%) in the colour composites. For a few points in time the comparison of Wolkam images with the false colour composites was not possible due to the low sun elevation. The CDA adapted to SEVIRI detected 7 contrails (9%). Comparing the automated contrail detection with the best visual inspection results (temperature difference images) yields a detection

efficiency of 58%. These results are shown in Table 3 as a function of contrail width.

The detection efficiency in brightness temperature and false colour images between 9–15% is significantly lower than those of the comparable AVHRR tools, the CDA efficiency is of equal magnitude. Only the CDA detection efficiency when compared to brightness temperature differences is higher and almost reaches 60%. The analysis of contrail widths was not executed due to the lower number of contrails observed in SEVIRI images. The low efficiency is caused by the low resolution of the SEVIRI infrared channels being 3 km/pixel in contrast to 1.1 km/pixel of AVHRR, this difference is enhanced by SEVIRI's slant view on Central Europe. Notice that the majority of investigated contrails has a width that is smaller than SEVIRI's spatial resolution. Nonetheless, even contrails featuring widths of less than 1 km were sporadically visible or detected by the CDA.

In the 2797 points in time processed during May 2007, the CDA detected contrail pixels in 299 cases, i.e. 11% of the time. The frequency obtained by Wolkam data is 31%, nearly three times as high. However this percentage cannot be directly compared to the MSG/SEVIRI values because only daylight hours and times of visible cirrus level could be used. The frequency averaged over all hours should be somewhat lower due to lower nocturnal contrail coverage (Mannstein et al., 1999). The remaining difference is probably caused by thin contrails which cannot be detected in SEVIRI imagery. At 103 of the mentioned 299 points in time the cirrus level was visible in Wolkam images making the comparison of the CDA results to ground-based imagery possible, in 28 cases (27%) the contrails marked by the CDA were identical to contrails photographed by the all-sky camera. In most of the remaining cases the CDA marked elongated, some 10 km wide cirrus streaks that are not identified as contrails in the visual interpretation of the Wolkam images. Some of them might have been induced by air traffic, but are in a later stage of their evolution into contrail cirrus. This kind of clouds is known to be responsible for most misdetections generated by the AVHRR version of the CDA (Mannstein et al., 1999).

6.2 Validation of MeCiDA cirrus diurnal cycles: April – September 2007

The analysis of the distribution of cirrus occurrence during the day obtained by MeCiDA from April to September 2007 over the Wolkam location as described in Sect. 3.3 yields a slight diurnal cycle featuring a 69% minimum at 09:00 UTC and a 76% maximum at 21:00 UTC, between these times there is a gentle increase during daytime and an almost as gentle decrease during nighttime, both of them are not monotone (Fig. 7).

The Wolkam camera enabled to analyse the diurnal cycle of ice clouds between 04:00 UTC (04:00–05:00 UTC) and 18:00 UTC (18:00–19:00 UTC). In Fig. 7 the occurrence of the "All ice clouds" is plotted because it is rather comparable to satellite data that cannot distinguish between contrails and cirrus. A rise of the cirrus frequency from 30% at 04:00 UTC to 51% at 17:00 UTC is visible. Both diurnal cycles have in common that this frequency is larger in the evening than in the morning hours, but the daytime increase gained from Wolkam is remarkably more pronounced. The fact that the values obtained by MeCiDA are considerably higher has various reasons: 1) MeCiDA does not only detect (thin) cirrus but also icy tops of high reaching convective clouds that Wolkam classifies as "Low- and medium-level clouds"; 2) the classification of cloud type in the poorly observable parts of the camera images close to the horizon is difficult, especially when a low cloud above the camera location is present; 3) the region observed with SEVIRI is somewhat larger and the probability of cirrus occurrence increases; 4) MeCiDA seems to often classify single isolated pixels as cloudy although no large scale cirrus pattern is visible in the surroundings.

The diurnal cycle of MeCiDA cirrus cloud coverage features a 40% minimum at 05:00 UTC and a 52% maximum at 18:00 UTC, in between there is a largely monotone rise respectively descent (Fig. 7). The coincidence of the absolute values (almost always closer than 5%) of the diurnal cycle of MeCiDA cirrus cloud coverage and the diurnal cycle of Wolkam "All ice clouds" occurrence is incidental, but the common trend of both curves, i.e. their increase during the day, is related: when cirrus cover increases, its probability of occurrence inside the all-sky camera field of view increases as well.

AMTD
2, 3183–3220, 2009

This feature is also observed in the month of July 2007 (and probably in other months as well).

A similar behaviour is shown in Stubenrauch et al. (2006): They extracted from the TOVS Path-B dataset diurnal cycles of high cloud amount in summer over northern midlatitudes land showing increases from 30% in the morning to 40% in the afternoon.

At times of low sun elevation the sky in Wolkam data appears more palish than otherwise and cirrus detection is more difficult. However, this reduced visibility of cirrus clouds at these times obviously does not induce a systematic error because the difference of the two graphs depicting relative frequencies in Fig. 7 are not symmetric with respect to noontime (11:00 UTC). The improved visibility of thin cirrus before sunrise and after sunset is also noticeable in Wolkam images, but this effect has no influence on the analysis as the period between sunset and sunrise is not considered in the data evaluation.

7 Conclusions and outlook

In contrast to satellite observations all-sky cameras feature high spatial and temporal resolution, thus nearly all contrails can be detected by visual inspection in a limited area around the camera location. Thus, they qualify as excellent instruments for the validation of satellite algorithms.

The analysis of the six months Wolkam time series (April – September 2007) revealed that contrails can be seen from ground 12% of the time, cirrus clouds 20%. The frequency with respect to the period with visible cirrus level are 21% for contrails and 35% for cirrus, with considerable variations between the months. The frequency of contrail occurrence does not vary significantly during daylight time. In contrast, cirrus clouds show a distinct diurnal cycle: their relative frequency of occurrence namely rises from 27% to 48% during daylight hours with respect to the time span characterised by visible cirrus level. The comparison of this frequency to the one gained by MeCiDA data indicates that MeCiDA is notedly higher at all hours of the day. However, when

looking at cirrus cloud cover from MeCiDA, a similar increase is found. This could be a hint that contrails with a lifetime of some hours evolve into cirrus clouds and cause the diurnal increase observed, but is more likely caused by convection.

Around 42% of the contrails identified in Wolkam images at the times of NOAA/AVHRR satellite overpasses could be recognised in channel 5 temperature and channel 4 – channel 5 temperature difference images, only 24% were identifiable in AVHRR colour composites, the CDA detected 8%. The percentage of contrails detected in AVHRR images increases with their width, but decreases with widths of more than 5 km, except for channel 5 temperatures. Regarding the contrails featuring widths of 1 to 5 km, detection efficiency of temperature and temperature difference images is 60–65%, 17% is the detection efficiency of the CDA. In order to compare with the detection efficiency (30–50%) from Mannstein et al. (1999), one must juxtapose visually detected AVHRR contrails and CDA contrails. In this case, the CDA detects approx. 28% of the contrails.

As far as contrail detection in MSG/SEVIRI is concerned, 79 contrails were visible, 15% of these could be identified in temperature difference images, 10% in the colour composites, the CDA detected 9%. This shows a worse detection than with AVHRR, due to the coarser spatial resoltion. During May 2007 the CDA yielded a 11% contrail frequency within the area observed by the Wolkam camera. During the periods of visible cirrus level, Wolkam images confirmed 27% of the CDA contrails and showed a high false alarm rate of the SEVIRI version of the CDA, mainly produced by elongated cirrus structures.

To achieve a substantially improved estimation of the climatic impact of contrails, an upgraded all-sky camera system allowing for an automated image interpretation is necessary. With the current system automated analysis was not feasible due to reflections, blurring and a large area affected by blooming caused by the sun. Besides a sensor with higher resolution the new system should feature a device to block direct sunlight from the dome. Furthermore it is important that the new camera system is able to operate during nighttime (such a system is described in Seiz et al. (2007)). Additionally

the acrylic dome should be heated to obtain time series without interruptions due to dew and rime. The utilisation of a camera system which is calibrated with respect to brightness temperature differences may enable the estimation of optical thickness by using the contrast between contrail and surrounding sky. The employment of two all-sky cameras would allow for the calculation of contrail height. Although, despite of all mentioned improvements, the creation of complete time series will not be possible due to the occurrence of clouds below the cirrus level, these improvements would offer the possibility to improve the understanding of the contrail-induced climatic effects by exploiting the full potential of all-sky cameras.

Acknowledgements. We thank EUROCONTROL and Kaspar Graf (DLR) for the provision of air traffic data, and Simon Unterstrasser for careful reading of the manuscript and valuable comments.

References

Appleman, H.: The formation of exhaust contrails by jet aircraft, B. Am. Meteorol. Soc., 34, 14–20, 1953. 3185

Bakan, S., Betancor, M., Gayler, V., and Grassl, H.: Contrail frequency over Europe from NOAA-satellite images, Ann. Geophys., 12, 962–968, 1994, http://www.ann-geophys.net/12/962/1994/. 3201

Fichter, C., Marquart, S., Sausen, R., and Lee, D.: The impact of cruise altitude on contrails and related radiative forcing, Meteorol. Z., 14(4), 563–572, 2005. 3193

Forster, P., Ramaswamy, V., Artaxo, P., Berntsen, T., Betts, R., Fahey, D., Haywood, J., Lean, J., Lowe, D., Myhre, G., Nganga, J., Prinn, R., Raga, G., Schulz, M., and Van Dorland, R.: Changes in atmospheric constituents and in radiative forcing, in: Climate change 2007: The physical science basis, Technical Report 2007, Intergovernmental Panel on Climate Change (IPCC), IPCC Secretariat, c/o World Meteorological Organization, Geneva, Switzerland, http://www.ipcc.ch, 2007. 3186

Gierens, K. M., Kärcher, B., Mannstein, H., and Mayer, B.: Aerodynamic contrails: Phenomenology and flow physics, J. Atmos. Sci., 66, 217–226, doi:10.1175/2008JAS2767.1, 2009. 3185

Goodrum, G., Kidwell, K., and Winston, E. W.: NOAA-KLM user's guide, Technical report, NOAA/NESDIS, National Climatic Data Center, 151 Patton Ave., Asheville, NC 28801-5001, http://www2.ncdc.noaa.gov/docs/klm/index.htm, 2003. 3189

Hahn C. and Warren, S.: A gridded climatology of clouds over land (1971–96) and ocean (1954–97) from surface observations worldwide, Numeric Data Package NDP-026E ORNL/CDIAC-153, CDIAC, Department of Energy, Oak Ridge, Tennessee, 2007. 3195

Inoue, T.: On the temperature and effective emissivity determination of semi-transparent cirrus clouds by bi-spectral measurements in the 10 μm window region, J. Meteorol. Soc. Jpn., 63(1), 88–99, 1985. 3192

IPCC: Climate change 2007: The scientific basis, Technical report, Intergovernmental Panel on Climate Change (IPCC), IPCC Secretariat, c/o World Meteorological Organization, Geneva, Switzerland, 2007. 3186

Jin, Y., Rossow, W., and Wylie, D.: Comparison of the climatologies of high-level clouds from HIRS and ISCCP, J. Climate, 9, 2850–2879, 1996. 3195

Krebs, W., Mannstein, H., Bugliaro, L., and Mayer, B.: Technical note: A new day- and night-time Meteosat Second Generation Cirrus Detection Algorithm MeCiDA, Atmos. Chem. Phys., 7, 6145–6159, 2007, http://www.atmos-chem-phys.net/7/6145/2007/. 3187, 3194

Kärcher, B., Mayer, B., Gierens, K., Burkhardt, U., Mannstein, H., and Chatterjee, R.: Aerodynamic contrails: Microphysics and optical properties, J. Atmos. Sci., 66, 227–243, doi:10.1175/2008JAS2768.1, 2009. 3185

Lee, D., Fahey, D., Forster, P., Newton, P., Wit, R., Lim, L., Owen, B., and Sausen, R.: Aviation and global climate change in the 21st century, Atmos. Environ., 53, 3520–3537, 2009. 3186

Mannstein, H., Meyer, R., and Wendling, P.: Operational detection of contrails from NOAA-AVHRR-data, Int. J. Remote Sens., 20(8), 1641–1660, 1999. 3185, 3186, 3191, 3193, 3200, 3203, 3206

Marquart, S.: Klimawirkung von Kondensstreifen: Untersuchungen mit einem globalen atmosphärischen Zirkulationsmodell, Dissertation, Fakultät für Physik der Ludwig-Maximilians-Universität München, 2003. 3185

Meerkötter, R., Schumann, U., Doelling, D. R., Minnis, P., Nakajima, T., and Tsushima, Y.: Radiative forcing by contrails, Ann. Geophys., 17, 1080–1094, 1999, http://www.ann-geophys.net/17/1080/1999/. 3185

Meyer, R., Mannstein, H., Meerkötter, R., Schumann, U., and Wendling, P.: Regional radiative forcing by line-shaped contrails derived from satellite data, J. Geophys. Res., 107(D10), 4104, doi:10.1029/2001JD000426, 2002. 3185, 3186, 3193, 3199, 3202

Minnis, P., Young, D., Garber, D., Nguyen, L., Smith Jr., W., and Palikonda, R.: Transformation of contrails into cirrus during SUCCESS, Geophys. Res. Lett., 25, 1157–1160, 1998. 3185

Minnis, P., Ayers, J., Palikonda, R., and Phan, D.: Contrails, cirrus trends, and climate, J. Climate, 17, 1671–1685, 2004. 3185

Minnis, P., Palikonda, R., Walter, B. J., Ayers, J. K., and Mannstein, H.: Contrail properties over the eastern North Pacific from AVHRR data, Meteorol. Z., 14(4), 515–523, doi:10.1127/0941–2948/2005/0056, 2005. 3186

Sassen, K.: Contrail-cirrus and their potential for regional climate change, B. Am. Meteorol. Soc., 78, 1885–1903, 1997. 3187

Sausen, R., Gierens, K., Ponater, M., and Schumann, U.: A diagnostic study of the global distribution of contrails: Part I: Present day climate, Theor. Appl. Climatol., 61, 127–141, 1998. 3201

Schmetz, J., Pili, P., Tjemkes, S., Just, D., Kerkmann, J., Rota, S., and Ratier, A.: An introduction to Meteosat Second Generation (MSG), B. Am. Meteorol. Soc., 83(7), 977–992, 2002. 3188

Schmidt, E.: Die Entstehung von Eisnebel aus den Auspuffgasen von Flugmotoren, Schriften der Deutschen Akademie der Luftfahrtforschung, 44, 1–15, 1941. 3184, 3185

Schumann, U.: On conditions for contrail formation from aircraft exhausts, Meteorol. Z., 5, 4–23, 1996. 3185

Schumann, U.: Formation, Properties and Climate Effects of Contrails, C. R. Phys., 6, 549–565, 2005. 3184, 3185, 3186

Scott, N., Chèdin, A., Armante, R., Francis, J., Stubenrauch, C. J., Chaboureau, J.-P., Chevallier, F., Claud, C., and Chèruy, F.: Characteristics of the TOVS Pathfinder Path-B Dataset, B. Am. Meteorol. Soc., 80, 2679–2701, 1999. 3195

Seiz, G., Shields, J., Feister, U., Baltsavias, E., and Gruen, A.: Cloud mapping with ground-based photogrammetric cameras, Int. J. Remote Sens., 28(9), 2001–2032, 2007. 3206

Stordal, F., Myhre, G., Stordal, E. J. G., Rossow, W. B., Lee, D. S., Arlander, D. W., and Svendby, T.: Is there a trend in cirrus cloud cover due to aircraft traffic?, Atmos. Chem. Phys., 5, 2155–2162, 2005, http://www.atmos-chem-phys.net/5/2155/2005/. 3186

Stubenrauch, C., Chèdin, A., Rädel, G., Scott, N., and Serrar, S.: Cloud Properties and Their Seasonal and Diurnal Variability from TOVS Path-B, J. Climate, 19, 5531–5553, 2006. 3205
Stuber, N. and Forster, P.: The impact of diurnal variations of air traffic on contrail radiative forcing, Atmos. Chem. Phys., 7, 3153–3162, 2007, http://www.atmos-chem-phys.net/7/3153/2007/. 3185
Trepte, S. and Winkler, P.: Langfristige meteorologische Veränderungen und UV-Strahlung, Ozonbulletin 81, Deutscher Wetterdienst, Offenbach am Main, 2001. 3196
Wylie, D. and Wang, P.: Comparison of cloud frequency data from HIRS and SAGE II, J. Geophys. Res., 102, 29893–29900, 1997. 3195
Wylie, D., Jackson, D., Menzel, W., and Bates, J.: Trends in Global Cloud Cover in Two Decades of HIRS Observations, J. Climate, 18, 3021–3031, 2005. 3195
Zerefos, C. S., Eleftheratos, K., Balis, D. S., Zanis, P., Tselioudis, G., and Meleti, C.: Evidence of impact of aviation on cirrus cloud formation, Atmos. Chem. Phys., 3, 1633–1644, 2003, http://www.atmos-chem-phys.net/3/1633/2003/. 3186

Table 1. AVHRR/3 (NOAA18) and SEVIRI channel numbers and effective channel central wavelengths λ_c.

AVHRR/3												
Channel	1	2	3A	3B					4	5		
λ_c/μm	0.63	0.85	1.61	3.76					10.77	12.00		
SEVIRI												
Channel	1	2	3	4	5	6	7	8	9	10	11	12
λ_c/μm	0.64	0.81	1.64	3.92	6.25	7.35	8.70	9.66	10.8	12.0	13.4	0.75

Table 2. Comparison of contrail detection in Wolkam and NOAA/AVHRR data as a function of their width.

Width (km)	<0.5	0.5–0.9	1.0–1.9	2.0–4.9	≥5.0	total
Wolkam	21	21	33	14	7	96
Channel 5	0	5	19	9	5	38
Temp. difference	1	9	20	9	1	40
Colour composite	0	3	12	7	1	23
CDA	0	0	5	3	0	8

Table 3. Comparison of contrail detection in Wolkam and MSG/SEVIRI data as a function of their width.

Width (km)	<0.5	0.5–0.9	1.0–1.9	2.0–4.9	≥5.0	total
Wolkam	29	27	14	7	2	79
Temp. difference	0	2	6	4	0	12
Colour composite	0	0	1	4	2	7
CDA	0	1	2	2	2	7

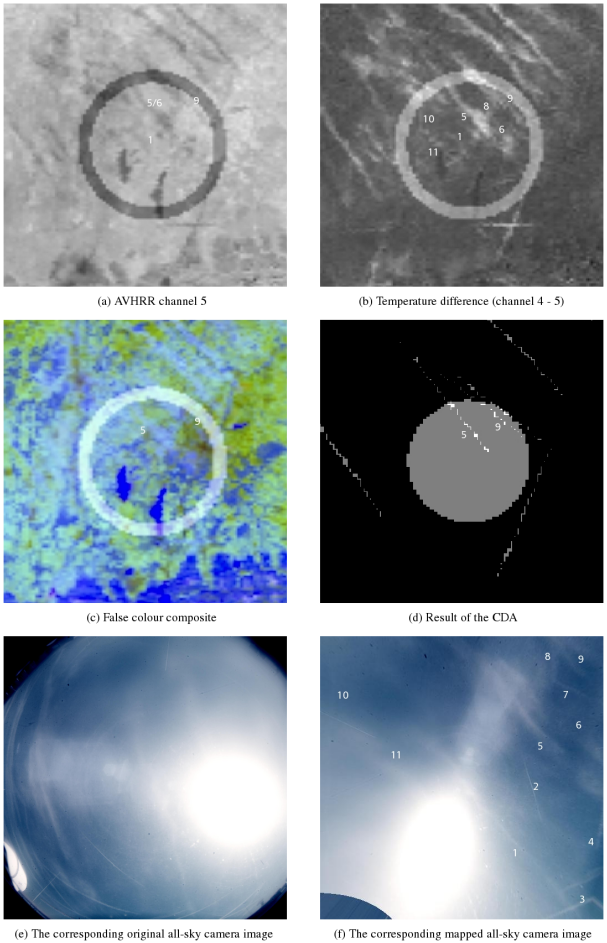

Fig. 1. Contrail scene of 16 April 2007, 12:02 UTC. All the used image types gained from AVHRR data and the result of the CDA are shown together with the corresponding Wolkam picture.

AMTD
2, 3183–3220, 2009

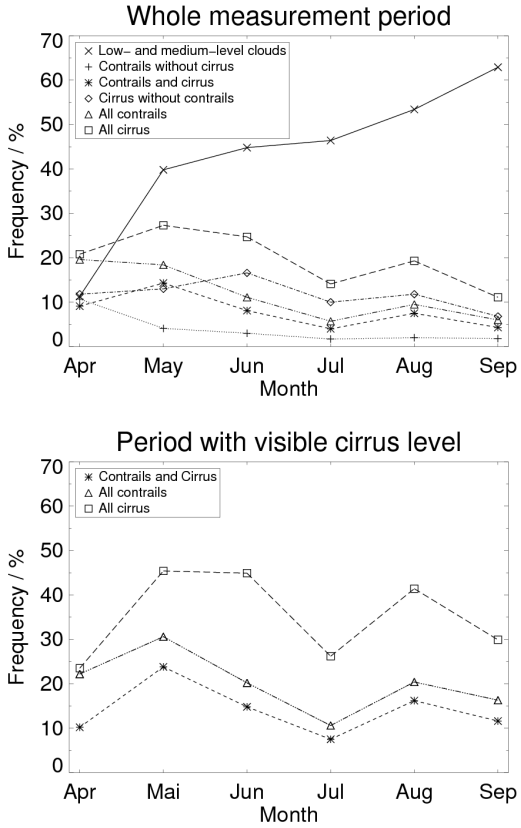

Fig. 2. Monthly mean values for the visual classification of ground based images. Left: Frequency of the occurrence of the categories "Low- and medium-level clouds" (×), "Contrails without cirrus" (+), "Contrails and cirrus" (∗), "Cirrus without contrails" (◊), "All contrails" (△), and "All cirrus" (□). Right: Frequency of occurrence of the categories "Contrails and cirrus" (∗), "All contrails" (△) and "All cirrus" (□) when the cirrus level was visible.

AMTD
2, 3183–3220, 2009

Title Page
Abstract Introduction
Conclusions References
Tables Figures
◀I ▶I
◀ ▶
Back Close
Full Screen / Esc
Printer-friendly Version
Interactive Discussion

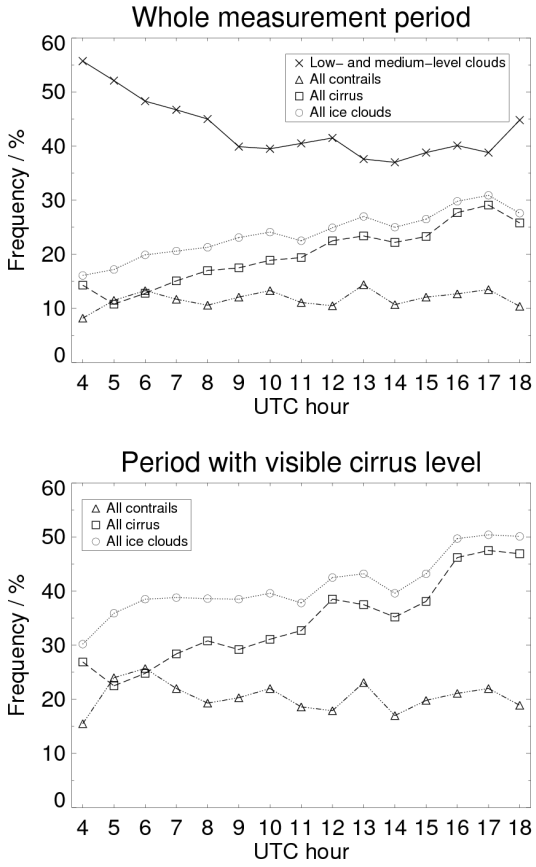

Fig. 3. Left: Frequency of occurrence of the categories “Low- and medium-level clouds” (×), “All contrails” (△), “All cirrus” (□) and “All ice clouds” (○), w.r.t. the full measurement period. Right: Frequency of occurrence of the categories “All contrails” (△), “All cirrus” (□) and “All ice clouds” (○), w.r.t. the time when the cirrus level was visible from the ground.

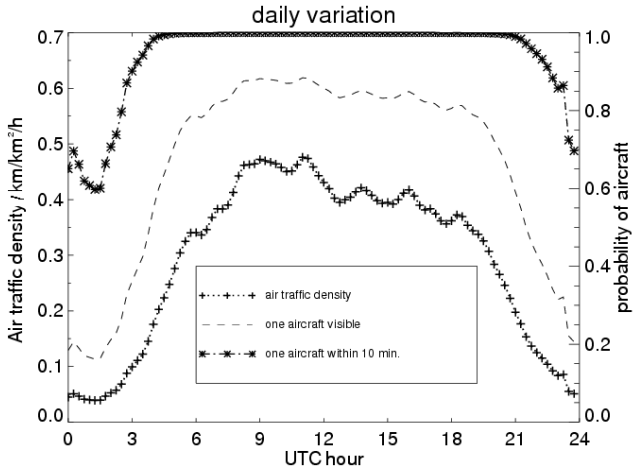

Fig. 4. Daily variation of higher level air traffic density (flown distance per square km and hour) in Southern Bavaria according to data from EUROCONTROL for the summer schedule of 2004 (+); probability that at least one aircraft is within Wolkam's field of view (dashed line); probability that at least one aircraft is visible in Wolkam's field of view within 10 min (∗).

AMTD
2, 3183–3220, 2009

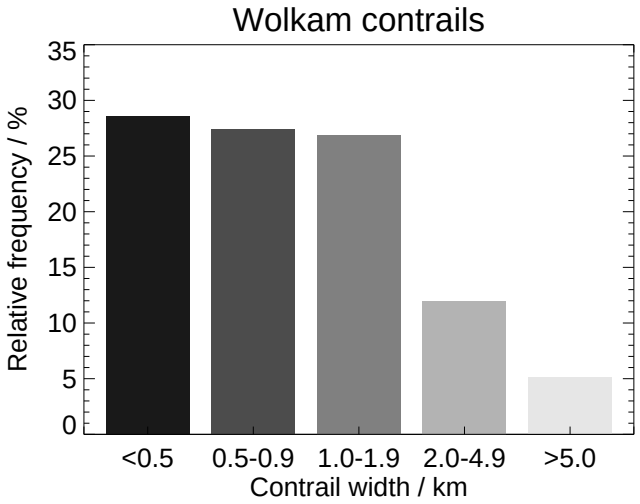

Fig. 5. Width distribition of 175 contrails observed using the all-sky camera.

AMTD
2, 3183–3220, 2009

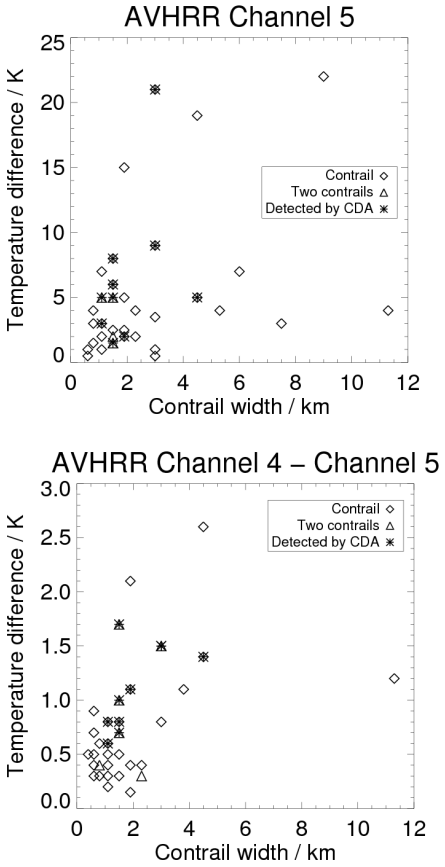

Fig. 6. Left: Relationship of contrail width and brightness temperature difference between the contrail and its surrounding in AVHRR channel 5. Right: Relationship of contrail width and brightness temperature difference between the contrail and its surrounding in the temperature difference image (channel 4–5). Diamonds (◊) mark single contrails detected in AVHRR data, triangles (△) indicate 2 contrails each, an asterisk (∗) at the centre marks the successful detection of the contrail by the CDA.

AMTD
2, 3183–3220, 2009

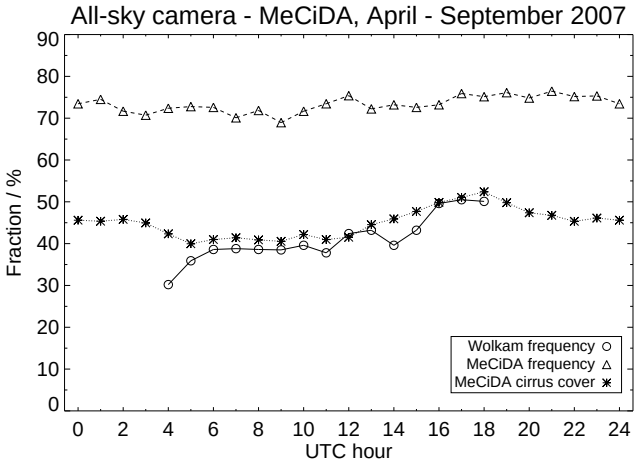

Fig. 7. Diurnal cycles of the frequency of "All ice clouds" occurrence obtained from all-sky camera data (◯) and via the MeCiDA algorithm (△) and the diurnal cycle of cirrus cloud coverage gained from MeCiDA (∗).

AMTD
2, 3183–3220, 2009